A large role of missing volatile organic compounds reactivity from anthropogenic emissions in ozone pollution regulation

Wenjie Wang[1,2]*, Bin Yuan[1]*, Hang Su[2], Yafang Cheng[2], Jipeng Qi[1], Sihang Wang[1], Wei Song[3], Xinming Wang[3], Chaoyang Xue[2], Chaoqun Ma[2], Fengxia Bao[2], Hongli Wang[4], Shengrong Lou[4], Min Shao[1]

[1] Institute for Environmental and Climate Research, Jinan University, Guangzhou 511443, China

[2] Multiphase Chemistry Department, Max Planck Institute for Chemistry, Mainz 55128, Germany

[3] State Key Laboratory of Organic Geochemistry, Guangzhou Institute of Geochemistry, Chinese Academy of Sciences, Guangzhou 510640, China

[4] State Environmental Protection Key Laboratory of Formation and Prevention of Urban Air Pollution Complex, Shanghai Academy of Environmental Sciences, Shanghai 200233, China

Correspondence to: Bin Yuan (byuan@jnu.edu.cn);
                   Wenjie Wang (Wenjie.Wang@mpic.de)

Abstract: There are thousands of VOC species in ambient air, while existing techniques can only detect a small part of them (~ several hundred). The large number of unmeasured VOCs prevents us from understanding the photochemistry of ozone and aerosols in the atmosphere. The major sources and photochemical effects of these unmeasured VOCs in urban areas remain unclear. The missing VOC reactivity, which is defined as the total OH reactivity of the unmeasured VOCs, is a good indicator to constrain the photochemical effect of unmeasured VOCs. Here, we identified the dominant role of anthropogenic emission sources in the missing VOC reactivity (accounting for up to 70%) by measuring missing VOC reactivity and tracer-based source analysis in a typical megacity in China. Omitting the missing VOC reactivity from anthropogenic emissions in model simulations will remarkably affect the diagnosis of sensitivity regimes for ozone formation, overestimating the degree of VOC-limited regime by up to 46%. Therefore, a thorough quantification of missing VOC reactivity from various anthropogenic emission sources is urgently needed for constraints of air quality models and the development of effective ozone control strategies.

1 Introduction

Volatile organic compounds (VOCs) are key precursors of major photochemical pollutants, including ozone (O_3) and secondary organic aerosols(Atkinson, 2000;Atkinson and Arey, 2003). Severe O_3 and particle pollution are frequently related to high emissions of VOCs (Atkinson and Arey, 2003;Monks et al., 2015). There exist thousands of VOC species in ambient air that are emitted from either natural processes or anthropogenic activities (Goldstein and Galbally, 2007). No one instrument can capture all VOCs out there and even when they can be measured there is information missing on identification and properties (Yuan et al., 2017;Wang et al., 2014). Gas chromatograph–mass spectrometer/flame ionization detector (GC–MS/FID) can measure C2-C12 non-methane hydrocarbons (NMHCs) and C2-C6 oxygenated VOCs (OVOCs) while cannot measure NMHCs and OVOCs with larger carbon number (Wang et al., 2014). Proton-transfer-reaction time-of-flight mass spectrometer (PTR-ToF-MS) is able to measure a huge number of OVOCs and aromatics and several alkanes, but cannot measure most alkanes and alkenes, and cannot distinguish isomers (Yuan et al., 2017). The 2,4-dinitrophenylhydrazine (DNPH)/high performance liquid chromatography (HPLC) method can measure several carbonyls but cannot measure non-polar organic species (Wang et al., 2009). The two-dimensional GC is able to measure some intermediate-volatile and semi-volatile non-polar organics (Song et al., 2022). A lack of standard gases prevents these technologies from accurate quantification even if these technologies can identify more VOC species. In general, many branched alkenes, OVOCs with complex functional groups, intermediate-volatile and semi-volatile organics and complex biogenic VOCs cannot currently be well quantified even if they can be identified by instruments. As a result, the total amount of VOCs in ambient air has generally been underestimated. Currently, emission inventories used in air quality models such as the Community Emissions Data System (CEDS) emission inventory and the multi-resolution Emission Inventory for China (MEIC) only include the VOC species that can be measured such as some C1-C9

hydrocarbons and simple-structure OVOCs with small carbon number (<C6). This will lead to an underestimation of the photochemical effect of total VOCs and thus causes uncertainties in predicting secondary pollution. The quantification of the unmeasured VOCs is crucial to assess secondary pollution precisely.

The total OH reactivity (R_{OH}), which can be directly measured, is an index for evaluating the amount of reductive pollutants in terms of ambient OH loss. The total OH reactivity is defined as:

$$R_{OH} = \sum_i k_{OH+Xi} [X_i], \qquad (1)$$

where X represents a reactive species including carbon monoxide (CO), nitrogen oxides (NO$_X$) and VOCs etc., and k_{OH+Xi} is the reaction rate constant for the oxidation of species X by OH. The measured R_{OH} is higher than that calculated based solely on the measured reactive species, and the difference between them is mostly from unmeasured VOCs (Yang et al., 2017). Missing VOC reactivity (missing VOC$_R$), defined as VOC reactivity (VOC$_R$) of all unmeasured VOCs, can be obtained by subtracting the calculated R_{OH} from the measured R_{OH}.

$$missing\ VOC_R = measured\ R_{OH} - calculated\ R_{OH} \qquad (2)$$

$$calculated\ R_{OH} = \sum_i k_{OH+reactive\ species_i} [reactive\ species_i] \qquad (3)$$

where reactive species represents measured VOCs and reactive inorganic species including carbon monoxide (CO), nitric oxide (NO), nitrogen dioxide (NO$_2$), O$_3$, sulfur dioxide (SO$_2$), nitrous acid (HONO), and so on. The missing VOC$_R$ provides a constraint for evaluating the photochemical roles of unmeasured VOCs in the atmosphere (Sadanaga et al., 2005;Yang et al., 2016b). The inclusion of the missing VOC$_R$ can help to improve the performance of box model and air quality models in simulating photochemistry processes. Relatively high missing VOC$_R$ have been found in forests (Di Carlo et al., 2004;Hansen et al., 2014;Nakashima et al., 2014;Nölscher et al., 2016;Praplan et al., 2019), urban areas (Shirley et al., 2006;Yoshino et al., 2006;Dolgorouky et al., 2012;Yang et al., 2017) and suburban areas (Kovacs et al., 2003;Yang et al., 2017;Fuchs et al., 2017;Lou et al., 2010), accouting for 10-75% of total R_{OH}. Given that total VOC$_R$ is one part of total R_{OH}, missing VOC$_R$ would account

95   for a larger percentage of total VOC_R (>10%-75%).

96   The potential sources of missing VOC_R include anthropogenic emissions, biogenic

97   emissions, soil emissions, and photochemical production, etc (Yang et al., 2016b).

98   Previous studies have reported that the missing VOC_R in forest areas was mainly from

99   either direct emissions or photochemical oxidation of biogenic VOCs (Di Carlo et al.,

100   2004;Hansen et al., 2014;Nakashima et al., 2014;Nölscher et al., 2016;Praplan et al.,

101   2019). Nevertheless, the dominant source of the missing VOC_R in urban and suburban

102   areas remains unclear or under debate.

103   Surface O_3 pollution has become a major public health concern in cities worldwide

104   (Paoletti et al., 2014;Lefohn et al., 2018). A critical issue in determining an emission

105   control strategy for ozone pollution is to understand the relative benefits of NOx and

106   VOC emission controls. This is generally framed in terms of ozone precursor sensitivity,

107   i.e., whether ozone production is NO_X-limited or VOC-limited (Kleinman,

108   1994;Sillman et al., 1990). Nevertheless, the effect of missing VOCs on ozone

109   precursor sensitivity has not been well understood yet. Given that the missing VOC_R

110   could potentially account for a large part of total VOC_R, clearly clarifying the role of

111   missing VOC_R in determining ozone precursor sensitivity is an urgent need for the

112   diagnosis of ozone sensitivity regimes and formulation of an effective emission

113   reduction roadmap.

114   China has become a global hot spot of ground-level ozone pollution in recent years

115   (Lu et al., 2018;Wang et al., 2022). Pearl River Delta (PRD) remains one of the most

116   O_3-polluted regions in China (Li et al., 2022), although many control measures have

117   been attempted. Here, we measured R_{OH} in Guangzhou, a megacity in PRD and

118   quantified the missing VOC_R. The dominant source of the missing VOC_R and its impact

119   on ozone precursor sensitivity were comprehensively investigated.

2 Method

2.1 Overview of the measurment

The field campaign was conducted from 25 September to 30 October 2018 continuously at an urban site in downtown Guangzhou (113.2ºE, 23ºN). The sampling site is located on the ninth floor of a building on the campus of Guangzhou Institute of Geochemistry, Chinese Academy of Sciences, 25 m above the ground level. This site is primarily influenced by industrial and vehicular emissions. ROH, VOCs, NOX, O3, HONO, SO2, CO, photolysis frequencies, and meteorological factors were simultaneously measured during the measurement period.

2.2 R_{OH} measurement

Total R_{OH} was measured by the comparative reactivity method (CRM) (Sinha et al., 2008). The CRM system consists of three major components, namely an inlet and calibration system, a reactor, and a measuring system. Here, pyrrole (C_4H_5N) was used as the reference substance in CRM and its concentration was quantified by a quadrupole proton-transfer-reaction mass spectrometer (PTR-MS) (Ionicon Analytik GmbH, Innsbruck, Austria). The CRM system was calibrated by propane, propene, toluene standards and 16 VOC mixed standard (acetaldehyde, methanol, ethanol, isoprene, acetone, acetonitrile, methyl vinyl ketone, methyl ethyl ketone, benzene, toluene, o-xylene, α-pinene, 1,2,4-trimethylbenzene, phenol, m-cresol, and naphthalene). Measured and calculated R_{OH} agreed well within 15% for all calibrations. The R_{OH} measurement by the CRM method is interfered from ambient nitric oxide (NO), which produces additional OH radicals via the reaction of HO_2 radicals with NO (Sinha et al., 2008). To correct this interference, a series of experiments were conducted by introducing different levels of NO (0–160 ppb) and given amounts of VOC into the CRM reactor. A correction curve was acquired from these NO interference experiments, which can be used to correct the R_{OH} thanks to the simultaneous measurement of

ambient NO concentrations (Supplementary information S1; Fig. S1). The detection limits of the CRM method were around 2.5 s^{-1}, and the total uncertainty was estimated to be about 15%. The CRM method has been successfully applied to measure OH reactivity in urban areas with high NO_X levels in previous studies (Dolgorouky et al., 2012;Yang et al., 2017;Hansen et al., 2015). The intercomparison between the CRM method and pump–probe technique indicates that the CRM method can be used under high-NO_X conditions (NO_X>10 ppb) if a NO_X -dependent correction is applied (Hansen et al., 2015).

2.3 VOCs measurements

Nonmethane hydrocarbons (NMHCs) were measured using a gas chromatograph–mass spectrometer/flame ionization detector (GC–MS/FID) system coupled with a cryogen-free preconcentration device (Wang et al., 2014). The system contains two-channel sampling and GC column separation, which is able to measure C2–C5 hydrocarbons with the FID in one channel and measure C5–C12 hydrocarbons using MS detector in the other channel. After removal of water vapor, VOCs were trapped at -155 ℃ in a deactivated quartz capillary column (15 cm×0.53 mm ID) and a Porous Layer Open Tubular (PLOT) capillary column (15 cm×0.53 mm ID) for the MS channel and the FID channel, respectively. The system was calibrated weekly by TO-15 (Air Environmental Inc., USA) and PAMS gas standards (Spectra Gases Inc., USA). Detection limits for various compounds were in the range of 0.002–0.070 ppbv. A total of 56 NMHCs species were measured (**Table S1**). The time resolution of the measurement was 1 h. The uncertainties of VOC measurements by GC–MS/FID are in the range of 15 %–20 %. More details of this method can be found in previous studies (Wang et al., 2014;Yuan et al., 2012).

An online proton-transfer-reaction time-of-flight mass spectrometer (PTR-ToF-MS) (Ionicon Analytic GmbH, Innsbruck, Austria) with H_3O^+ and NO^+ ion sources was also used to measure VOCs. During the campaign, the PTR-ToF-MS automatically switched between H_3O^+ and NO^+ chemistry every 10–20 min. The H_3O^+ mode was

174 used to measure OVOCs and aromatics while the NO^+ model was used to measure

175 alkanes with more carbons (C8-C20). When running in the H_3O^+ ionization mode, the

176 drift tube was at a temperature of 50 °C, a pressure of 3.8 mbar, and a voltage of 920

177 V, leading to an operating E/N (E is the electric field, and N is the number density of

178 the gas in the drift tube) ratio of 120 Td. When running in the NO^+ ionization mode, the

179 drift tube was at a temperature of 50 °C, a pressure of 3.8 mbar, and a voltage of 470

180 V, leading to an operating E/N ratio of 60 Td. PTR-ToF-MS technique is capable of

181 measuring oxygenated VOCs (OVOCs) and higher alkanes that GC–MS/FID cannot

182 measure (Wu et al., 2020;Wang et al., 2020a). The time resolution of PTR-ToF-MS

183 measurements was 10 s. A total of 31 VOCs were calibrated using either gas or liquid

184 standards (Table S2). For other measured VOCs, we used the method proposed by

185 Sekimoto et al. (2017) to determine the relationship between VOC sensitivity and

186 kinetic rate constants for proton transfer reactions of H_3O^+ with VOCs. The fitted line

187 was used to determine the concentrations of those uncalibrated species. The

188 uncertainties of the concentrations for uncalibrated species were about 50 % (Sekimoto

189 et al., 2017). By this metod, PTR-ToF-MS can additionally measure 128 VOCs which

190 were included in the analysis of this study. The detailed information for this method can

191 be found in Wu et al. (2020) and all VOC species measured by PTR-ToF-MS were

192 provided in table S4 of that article. The PTR-ToF-MS is capable of measuring

193 additional VOC species that GC–MS/FID cannot measure including alkanes with more

194 carbons (C12–C20) and OVOCs including aldehydes, ketones, carboxylic acids,

195 alcohols, and nitrophenols. Formaldehyde (HCHO) was measured by a custom-built

196 instrument based on the Hantzsch reaction and absorption photometry (Xu et al., 2022).

197 **2.4 Other measurements**

198 Nitrous acid (HONO) was measured by a custom-built LOPAP (Long Path

199 Absorption Photometer) based on wet chemical sampling and photometric detection

200 (Yu et al., 2022). The uncertainty of the measurement was 8 %. NO_X, O_3, SO_2, and CO

201 were measured by NO_X analyzer (Thermo Scientific, Model 42i), O_3 analyzer (Thermo

202 Scientific, Model 49i), SO_2 analyzer (Thermo Scientific, Model 43i), and CO analyzer

(Thermo Scientific, Model 48i), respectively. The meteorological data, including temperature (T), relative humidity (RH) and wind speed and direction (WS, WD) were recorded by Vantage Pro2 Weather Station (Davis Instruments Inc., Vantage Pro2) with a time resolution of 1 min. Photolysis frequencies of O_3, NO_2, HONO, H_2O_2, HCHO, and NO_3 were measured by a spectrometer (Focused Photonics Inc., PFS-100) (Shetter and Müller, 1999;Wang et al., 2019).

2.5 Multiple linear regression

The Multiple Linear Regression (MLR) has been successfully applied to quantify the sources of air pollutants (Li et al., 2019;Yang et al., 2016a). In this study, a tracer-based MLR analysis was used to decouple the individual contributions of anthropogenic emissions, secondary production, biogenic emissions and background level to missing VOC_R, as shown in Eq. (4).

$$Missing\ VOC_R = a\Delta CO + b[O_X] + c[isoprene_{initial}] + C_{background} \qquad (4)$$

where O_X is defined as O_3+NO_2. ΔCO, $[O_X]$ and $[isoprene_{initial}]$ are concentrations of tracers for anthropogenic emissions, secondary production and biogenic emissions, respectively. ΔCO is the relative change between ambient CO and background CO of 150 ppb (Wang et al., 2020a). $[isoprene_{initial}]$ represents the initial concentration of isoprene from biogenic emissions that has not undergone any photochemical reactions, which is calculated from observed isoprene and its photochemical products methyl vinyl ketone (MVK) and methacrolein (MACR) (Xie et al., 2008). $C_{background}$ indicates the background level of missing VOC_R. a, b, c and $C_{backgound}$ are fitted coefficients by the multiple linear regression.

2.6 Observation-based box model

A zero-dimensional box model coupled with the Master Chemical Mechanism (MCM) v3.3.1 chemical mechanism (Jenkin et al., 2003) was used to simulate the photochemical production of RO_X (RO_X=OH+HO_2+RO_2) radicals and O_3 during the field campaign. The model was constrained by the observations of meteorological

230 parameters, photolysis frequencies, VOCs, NO, NO_2, O_3, CO, SO_2, and HONO. The

231 model runs were performed in a time-dependent mode with a time resolution of 1 hour

232 and a spin-up of four days. A 24-h lifetime was introduced for all simulated species,

233 including secondary species and radicals, to approximately simulate dry deposition and

234 other losses of these species (Lu et al., 2013;Wang et al., 2020b). Sensitivity tests show

235 that this assumed physical loss lifetime has a relatively small influence on RO_X radicals

236 and ozone production rates.

237 Measured OVOCs such as HCHO, acetaldehyde and acetone were constrained in

238 the model and unmeasured OVOCs were simulated according to the photochemical

239 oxidation of NMHCs by OH radicals. RO_2, HO_2 and OH radicals were simulated by the

240 box model to calculate the net O_3 production rate ($P(O_3)$) and O_3 loss rate ($L(O_3)$) as

241 shown in Equations (5) and (6) as derived by Mihelcic et al. (2003)

242 $$P(O_3) = k_{HO_2+NO}[HO_2][NO] + \sum_i(k^i_{RO_2+NO}[RO_2^i][NO]) - k_{OH+NO_2}[OH][NO_2] - L(O_3)$$

243 $$(5)$$

244 $$L(O_3) = (\theta j(O^1D) + k_{OH+O_3}[OH] + k_{HO_2+O_3}[HO_2] + \sum_j(k^j_{alkene+O_3}[alkene^j]))[O_3]$$

245 $$(6)$$

246 where θ is the fraction of O^1D from ozone photolysis that reacts with water vapor, and

247 i and j represent the number of species of RO_2 and alkenes, respectively.

248 The box model was used to evaluate the impact of missing VOC_R on the O_3

249 production rate. In the base scenario, the box model was constrained by all measured

250 inorganic and organic gases but the missing VOC_R was not considered. To consider the

251 missing VOC_R in the box model, we additionally increased the concentration of

252 NMHCs to exactly compensate for the missing VOC_R by multiplying a factor, on the

253 basis of measured NMHC concentrations. We simulated four scenarios by increasing

254 the concentration of: (1) n-pentane, (2) ethylene, (3) toluene, (4) all measured 56

255 NMHCs. For the scenario of increasing all 56 NMHCs, concentrations of 56 NMHC

256 species were increased by multiplying the same factor. Given that the VOC_R of

257 unconstrained secondary products increases with the increase in the concentration of

258 NMHCs, several attempts of different values are needed to determine the increasing

259 factor.

3 Results and discussion

3.1 Quantification of missing VOC$_R$ during the campaign

Figure 1 shows the time series of measured R$_{OH}$, calculated R$_{OH}$ according to all measured reactive gases, and missing VOC$_R$ (the gap between measured and calculated R$_{OH}$) in Guangzhou. By using GC-MS/FID, we measured 56 NMHCs. By using PTR-ToF-MS, we measured 159 VOCs and 128 of them were difficult to be measured before. Besides the alkanes with carbons less than 12, PTR-ToF-MS can also measure alkanes with more carbons (C12–C20). With regard to OVOCs, not only common OVOC species including formaldehyde and C2-C4 carbonyls but also carbonyls with more carbons (C5–C10) and some N-containing OVOC species such as nitrophenol and methyl nitrophenol were measured by PTR-ToF-MS. Thanks to these additional measured VOCs, the measured R$_{OH}$ was close to the calculated R$_{OH}$ within 20% in most periods. In some periods the missing VOC$_R$ was negative, which is probably due to the uncertainty in the measurements of R$_{OH}$ and reactive gases. The negative missing VOC$_R$ primarily occurred in the afternoon (12:00–17:00) when the photochemistry was most active. Nevertheless, there were still some days exhibiting remarkable missing VOC$_R$. The days with missing VOC$_R$ of more than 25% of total R$_{OH}$, namely high missing-VOC$_R$ days, are indicated by yellow background in **Fig. 1a**. The largest missing VOC$_R$ occurred on October 15th, 16th, 25th and 26th, with average values of 16 s^{-1}. During the period of October 24th to 26th, the total R$_{OH}$ was highest and the missing VOC$_R$ was also relatively high among all days. **Figure 1b** shows the contribution of different species classifications to total R$_{OH}$ during high missing-VOC$_R$ days. Inorganic species, NMHCs and OVOCs account for 34%, 13% and 14% of total R$_{OH}$, respectively, with missing VOC$_R$ accounting for 39%. The fraction of missing VOC$_R$ (39%) during the high missing–VOC$_R$ days is comparable to measurements in Los Angeles 2010 (Griffith et al., 2016) and in Seoul 2016 (Sanchez et al., 2021).

286   We evaluated the uncertainty of the missing VOC_R. The uncertainty of the R_{OH}

287   measurement was 15%. In addition, according to reports of Jet Propulsion Laboratory

288   (Burkholder et al., 2020), reaction rate constants used for the calculation of R_{OH} in Eq

289   (3) have uncertainties of 5%–30%, depending on different species. We took the

290   uncertainties in the reaction rate constants and the measurements of all reactive gases

291   into account when calculating R_{OH}, according to error propagation. As a result, the

292   uncertainties in the missing VOC_R are 3.8 s^{-1} and 5.2 s^{-1} for the whole measurement

293   period and the high missing-VOC_R days, respectively. The average missing VOC_R

294   during the high missing-VOC_R days is 13 s^{-1}, which is significantly higher than the

295   uncertainty of 5.2 s^{-1}, suggesting that the missing VOC_R really exists during the high

296   missing-VOC_R days.

297

298   **3.2 The sources of missing VOC_R**

299   To explore the sources of missing VOC_R during the whole measurement period,

300   we investigated the correlation between missing VOC_R and tracers characterizing

301   primary emissions (CO, NO_X and NMHCs) and secondary production ($O_X \equiv O_3 + NO_2$

302   and formic acid). The correlation of missing VOC_R with CO, reactivity of NMHCs

303   ($NMHC_R$) and NO_X is moderate, with correlation coefficient (R) in the range of 0.47–

304   0.56 (**Fig. 2a and b, and Fig. S2**) while there is no significant correlation of missing

305   VOC_R with O_X and formic acid (**Fig. 2c and Fig. S2**). Furthermore, there is no

306   significant correlation between missing VOC_R and acetonitrile which is a tracer of

307   biomass burning (de Gouw et al., 2003; Wang et al., 2007) (**Fig. S2**), indicating that

308   biomass burning was not a major contributor to missing VOC_R during this campaign.

309   In terms of the diurnal variation, the missing VOC_R was higher in the morning (7:00–

310   10:00) and evening (18:00–22:00) when the anthropogenic emissions, especially

311   vehicle exhaust were intensive, and was lower in the afternoon when the

312   photochemistry was most active (**Fig. 2d**). The diurnal profile of missing VOC_R was

313   similar to those of CO, NO_X and $NMHC_R$. In contrast, the diurnal profiles of secondary

314 species including O_X, formic acid and acetic acid, which peaked in the afternoon,

315 evidently differ from the diurnal profile of missing VOC_R (**Fig. S3**). Further, we

316 investigated the influence of airmass aging on missing VOC_R. The ratio of ethylbenzene

317 to m,p-xylene was used to characterize the degree of air mass aging (De Gouw et al.,

318 2005;Yuan et al., 2013). A higher ratio of ethylbenzene to m,p-xylene corresponds to a

319 higher degree of air mass aging as the m,p-xylene has a larger reaction rate constant

320 (18.9×10^{-12} cm^3 $molecule^{-1}s^{-1}$) than ethylbenzene (7.0×10^{-12} cm^3 $molecule^{-1}s^{-1}$) when

321 reacting with the major oxidant - OH radicals. As shown in **Fig. 2e**, missing VOC_R

322 decreases with the ratio of ethylbenzene to m,p-xylene. Given that secondary

323 production generally increased with air mass aging, this result further demonstrates that

324 missing VOC_R was not caused by enhanced secondary production.

325 During the high missing- VOC_R days, the correlation coefficient for missing VOC_R

326 versus CO is 0.76 **(Fig. 3a)**, which is higher than that in the whole measurement period

327 (0.56) shown in **Fig. 2a**. We then quantify the sources of missing VOC_R during the high

328 missing- VOC_R days by applying MLR. The fitted coefficient a is 0.031 s^{-1} ppb^{-1}, b is

329 0.012 s^{-1} ppb^{-1}, c is 1.8 s^{-1} ppb^{-1} and $C_{background}$ is 1.3 s^{-1}. The coefficient of determination

330 (R^2) for the MLR is 0.68. As shown in **Fig. 3b,** anthropogenic emissions were the largest

331 contributor to missing VOC_R, accounting for 70% of missing VOC_R. Secondary

332 production, biogenic emissions and background contribution played a minor role in

333 missing VOC_R (13%, 7%, 10%, respectively). The parametric relationship between

334 missing VOC_R and relevant tracers established by MLR provides a valid approach to

335 estimate the missing VOC_R according to readily available gases including CO, O_X and

336 isoprene.

337 Although anthropogenic emissions are identified to be the major source of missing

338 VOC_R, which species dominantly contribute to the missing VOC_R remains unclear. A

339 potential source is the unmeasured branched alkenes for their high reactivity, previously

340 observed from vehicle exhaust (Nakashima et al., 2010) and gasoline evaporation

341 emissions (Wu et al., 2015). Another possible source is emitted OVOCs with a more

342 complex functional group that cannot be accurately measured. In addition, directly

343 emitted semi-volatile and intermediate volatility organic compounds are also possible

344 sources of missing VOC_R (Stewart et al., 2021).

345 **3.3 The impact of missing VOC_R on O_3 sensitivity regimes**

346 The reaction of OH with VOCs is key to the propagation and amplification of OH

347 radicals, thus determining the ozone production rate (Tonnesen and Dennis, 2000). The

348 box model was used to evaluate the impact of missing VOC_R on the O_3 production rate

349 during high missing-VOC_R days. The setting of model simulations for different

350 scenarios are depicted in Section 2.6. Under the base scenario, on average the measured

351 VOC_R of n-pentane, ethylene, toluene and all 56 NMHCs are 0.14 s^{-1}, 0.53 s^{-1}, 0.60 s^{-1}

352 and 4.6 s^{-1} respectively. To consider the missing VOC_R (on average of 13 s^{-1}) in the

353 model, four scenarios were simulated by additionally increasing n-pentane, ethylene,

354 toluene and 56 NMHCs by a factor of 70, 16, 13.3 and 1.9, respectively. These

355 increasing factors led to an additional increase in VOC_R of both NMHCs and

356 unconstrained secondary products, which exactly compensated for the missing VOC_R.

357 **Figure 4** shows the simulated $P(O_3)$ for the base scenario and the scenarios considering

358 missing VOC_R. The daytime average $P(O_3)$ under the scenarios considering missing

359 VOC_R is a factor of 1.5–4.5 for the results under the base scenario. The difference in

360 added species has a large effect on $P(O_3)$. Adding toluene causes a larger increase in

361 $P(O_3)$ than adding n-pentane or ethene, as toluene has a stronger ability to amplify the

362 production of radicals.

363 O_3 precursor sensitivity depends on the dominant loss pathways of RO_X radicals

364 ($RO_X=OH+HO_2+RO_2$). O_3 production is NO_X-limited if the self-reaction of peroxy

365 radicals (HO_2 and RO_2) dominates the RO_X sink, and VOC-limited if the reaction of

366 NO_2 with OH dominates (Kleinman et al., 1997;Kleinman et al., 2001). Accordingly,

367 the ratio of RO_X sink induced by $OH+NO_2$ reaction to the total rate of the two RO_X

368 sinks, i.e., L_N/Q, is used to identify O_3 sensitivity regimes. O_3 production is NO_X-

369 limited if L_N/Q is lower than 0.5, otherwise, it is VOC-limited (Kleinman et al., 1997).

370 $$L_N/Q = \frac{k_{OH+NO_2}[OH][NO_2]}{k_{HO_2+RO_2}[HO_2][RO_2]+k_{HO_2+HO_2}[HO_2][HO_2]+k_{OH+HO_2}[OH][HO_2]+k_{OH+NO_2}[OH][NO_2]}$$

371   (7)

372   As shown in **Fig. 5a**, under the base scenario, L_N/Q remained at a stable and high

373 level (>0.9) during the daytime when photochemical production of ozone occurs,

374 indicating O_3 production was VOC-limited. Under the scenarios considering missing

375 VOC_R, L_N/Q decreased significantly regardless of which VOC species was added,

376 compared to the base scenario. Adding toluene caused the largest decrease in L_N/Q,

377 followed by adding all measured NMHC species, adding the alkane and adding the

378 alkene. It is worth noting that adding toluene and all measured NMHC species caused

379 the L_N/Q to be close to 0.5 in the afternoon, indicating that the O_3 production shifted to

380 transitional or NO_X-limited regimes in these scenarios. **Fig. 5b** shows the changes in

381 radical sinks before and after considering missing VOC_R. All radical sinks including

382 self-reactions of peroxy radicals and $OH+NO_2$ reaction increased after considering

383 missing VOC_R. Nevertheless, the increased proportion of the self-reactions of peroxy

384 radicals was larger than that of $OH+NO_2$ reaction, leading to a decrease in L_N/Q and

385 thus a shift toward NO_X-limited regime.

386   **Figure 5c** shows the dependence of daily peak O_3 concentrations on NO_X

387 concentrations, which was calculated by the box model for the base scenario and the

388 scenario considering missing VOC_R. The NO_X concentration level corresponding to the

389 maximum of O_3 concentrations was determined. This NO_X concentration level reflects

390 the threshold to distinguish between VOC-limited and NO_X-limited regimes. The larger

391 threshold of NO_X represents a higher possibility of ozone production in NO_X limited

392 regime. The threshold of NO_X for the scenario considering missing VOC_R is 46% higher

393 than for the base scenario. Note that the uncertainty in missing VOC_R leads to 17%

394 uncertainty in the threshold of NO_X for the scenario considering missing VOC_R. Overall,

395 **Fig. 5** suggests that omitting the missing VOC_R will overestimate the degree of the

396 VOC-limited regime and thus overestimate the effect of VOCs abatement in reducing

397 ozone pollution, which in turn may mislead ozone control strategy.

3.4 Atmospheric implications

Although many previous studies have reported that photochemical production processes and biogenic emissions are important sources of missing VOC_R (Lou et al., 2010;Dolgorouky et al., 2012;Yang et al., 2017;Sanchez et al., 2021;Di Carlo et al., 2004), we find that anthropogenic emissions may dominate the missing VOC_R in urban regions. In zero-dimensional box models and three-dimensional chemistry-transport models, the input of VOCs emission information mainly contains well-studied simple-structure alkanes, alkenes and aromatics, while those unmeasured/unknown VOC species have been neglected. This will lead to biases in quantifying ozone production and diagnosing ozone sensitivity regimes. Our study demonstrates that the ambient measurement of R_{OH} at urban sites can provide quantification of missing VOC_R, which can be used in models to account for the missing VOC_R from anthropogenic emissions. In addition, the parametric equation of missing VOC_R derived from MLR method (Eq (4)) here can be used to estimate missing VOC_R according to measurements of CO, O_X and isoprene. Further study should try to parse the specific sources of the missing VOC_R, e.g., whether the missing VOC_R is from intermediate-volatility and semivolatile organic compounds emitted from vehicles or whether it is from some other sources. Furthermore, future studies can focus on direct measurements of missing VOC_R for various emission sources to develop a comprehensive emission inventory of missing VOC_R, which will help to improve O_3 pollution mitigation strategies.

Acknowledgement

This work was supported by the National Natural Science Foundation of China (grant No. , 42121004, 42275103, 42230701, 42175135). This work was also supported by Special Fund Project for Science and Technology Innovation Strategy of Guangdong Province (Grant No.2019B121205004).

References

Atkinson, R.: Atmospheric chemistry of VOCs and NOx, Atmos. Environ., 34, 2063-2101, 2000.

Atkinson, R., and Arey, J.: Atmospheric degradation of volatile organic compounds, Chemical reviews, 103, 4605-4638, 2003.

Burkholder, J., Sander, S., Abbatt, J., Barker, J., Cappa, C., Crounse, J., Dibble, T., Huie, R., Kolb, C., and Kurylo, M.: Chemical kinetics and photochemical data for use in atmospheric studies; evaluation number 19, Pasadena, CA: Jet Propulsion Laboratory, National Aeronautics and Space …, 2020.

De Gouw, J., Middlebrook, A., Warneke, C., Goldan, P., Kuster, W., Roberts, J., Fehsenfeld, F., Worsnop, D., Canagaratna, M., and Pszenny, A.: Budget of organic carbon in a polluted atmosphere: Results from the New England Air Quality Study in 2002, J. Geophys. Res.-Atmos., 110, 2005.

de Gouw, J. A., Warneke, C., Parrish, D. D., Holloway, J. S., Trainer, M., and Fehsenfeld, F. C.: Emission sources and ocean uptake of acetonitrile (CH3CN) in the atmosphere, J. Geophys. Res.-Atmos., 108, https://doi.org/10.1029/2002JD002897, 2003.

Di Carlo, P., Brune, W. H., Martinez, M., Harder, H., Lesher, R., Ren, X. R., Thornberry, T., Carroll, M. A., Young, V., Shepson, P. B., Riemer, D., Apel, E., and Campbell, C.: Missing OH reactivity in a forest: Evidence for unknown reactive biogenic VOCs, Science, 304, 722-725, 10.1126/science.1094392, 2004.

Dolgorouky, C., Gros, V., Sarda-Esteve, R., Sinha, V., Williams, J., Marchand, N., Sauvage, S., Poulain, L., Sciare, J., and Bonsang, B.: Total OH reactivity measurements in Paris during the 2010 MEGAPOLI winter campaign, Atmos. Chem. Phys., 12, 9593-9612, 10.5194/acp-12-9593-2012, 2012.

Fuchs, H., Tan, Z., Lu, K., Bohn, B., Broch, S., Brown, S. S., Dong, H., Gomm, S., Häseler, R., He, L., Hofzumahaus, A., Holland, F., Li, X., Liu, Y., Lu, S., Min, K. E., Rohrer, F., Shao, M., Wang, B., Wang, M., Wu, Y., Zeng, L., Zhang, Y., Wahner, A., and Zhang, Y.: OH reactivity at a rural site (Wangdu) in the North China Plain: contributions from OH reactants and experimental OH budget, Atmos. Chem. Phys., 17, 645-661, 10.5194/acp-17-645-2017, 2017.

Goldstein, A. H., and Galbally, I. E.: Known and unexplored organic constituents in the earth's atmosphere, Environ. Sci. Technol., 41, 1514-1521, 2007.

Griffith, S. M., Hansen, R., Dusanter, S., Michoud, V., Gilman, J., Kuster, W., Veres, P., Graus, M., de Gouw, J., and Roberts, J.: Measurements of hydroxyl and hydroperoxy radicals during CalNex-LA: Model comparisons and radical budgets, J. Geophys. Res.-Atmos., 121, 4211-4232, 2016.

Hansen, R. F., Griffith, S. M., Dusanter, S., Rickly, P. S., Stevens, P. S., Bertman, S. B., Carroll, M. A., Erickson, M. H., Flynn, J. H., Grossberg, N., Jobson, B. T., Lefer, B. L., and Wallace, H. W.: Measurements of total hydroxyl radical reactivity during CABINEX 2009 – Part 1: field measurements, Atmos. Chem. Phys., 14, 2923-2937, 10.5194/acp-14-2923-2014, 2014.

Hansen, R. F., Blocquet, M., Schoemaecker, C., Léonardis, T., Locoge, N., Fittschen, C., Hanoune, B., Stevens, P. S., Sinha, V., and Dusanter, S.: Intercomparison of the comparative reactivity method (CRM) and pump–probe technique for measuring total OH reactivity in an urban environment, Atmos. Meas. Tech., 8, 4243-4264, 10.5194/amt-8-4243-2015, 2015.

Jenkin, M. E., Saunders, S. M., Wagner, V., and Pilling, M. J.: Protocol for the development of the Master Chemical Mechanism, MCM v3 (Part B): tropospheric degradation of aromatic volatile organic compounds, Atmos. Chem. Phys., 3, 181-193, 10.5194/acp-3-181-2003, 2003.

Kleinman, L. I.: Low and high NOx tropospheric photochemistry, J. Geophys. Res.-Atmos., 99, 16831-16838, 1994.

Kleinman, L. I., Daum, P. H., Lee, J. H., Lee, Y. N., Nunnermacker, L. J., Springston, S. R., Newman, L., Weinstein-Lloyd, J., and Sillman, S.: Dependence of ozone production on NO and hydrocarbons in the troposphere, Geophys. Res. Lett., 24, 2299-2302, 1997.

Kleinman, L. I., Daum, P. H., Lee, Y. N., Nunnermacker, L. J., Springston, S. R., Weinstein-Lloyd, J., and Rudolph, J.: Sensitivity of ozone production rate to ozone precursors, Geophys. Res. Lett., 28, 2903-2906, 2001.

Kovacs, T., Brune, W., Harder, H., Martinez, M., Simpas, J., Frost, G., Williams, E., Jobson, T., Stroud, C., and Young, V.: Direct measurements of urban OH reactivity during Nashville SOS in summer 1999, Journal of Environmental Monitoring, 5, 68-74, 2003.

Lefohn, A. S., Malley, C. S., Smith, L., Wells, B., Hazucha, M., Simon, H., Naik, V., Mills, G., Schultz, M. G., and Paoletti, E.: Tropospheric ozone assessment report: Global ozone metrics for climate change, human health, and crop/ecosystem research, Elem. Sci. Anth., 6, 2018.

Li, K., Jacob, D. J., Liao, H., Shen, L., Zhang, Q., and Bates, K. H.: Anthropogenic drivers of 2013–2017 trends in summer surface ozone in China, Proc. National Acad. Sci., 116, 422-427, 2019.

Li, X.-B., Yuan, B., Parrish, D. D., Chen, D., Song, Y., Yang, S., Liu, Z., and Shao, M.: Long-term trend of ozone in southern China reveals future mitigation strategy for air pollution, Atmos. Environ., 269, 118869, 2022.

Lou, S., Holland, F., Rohrer, F., Lu, K., Bohn, B., Brauers, T., Chang, C., Fuchs, H., Häseler, R., and Kita, K.: Atmospheric OH reactivities in the Pearl River Delta–China in summer 2006: measurement and model results, Atmos. Chem. Phys., 10, 11243-11260, 2010.

Lu, K. D., Hofzumahaus, A., Holland, F., Bohn, B., Brauers, T., Fuchs, H., Hu, M., Haseler, R., Kita, K., Kondo, Y., Li, X., Lou, S. R., Oebel, A., Shao, M., Zeng, L. M., Wahner, A., Zhu, T., Zhang, Y. H., and Rohrer, F.: Missing OH source in a suburban environment near Beijing: observed and modelled OH and HO2 concentrations in summer 2006, Atmospheric Chemistry and Physics, 13, 1057-1080, 10.5194/acp-13-1057-2013, 2013.

Lu, X., Hong, J. Y., Zhang, L., Cooper, O. R., Schultz, M. G., Xu, X. B., Wang, T., Gao, M., Zhao, Y. H., and Zhang, Y. H.: Severe Surface Ozone Pollution in China: A Global Perspective, Environ. Sci. Technol. Lett., 5, 487-494, 10.1021/acs.estlett.8b00366, 2018.

Mihelcic, D., Holland, F., Hofzumahaus, A., Hoppe, L., Konrad, S., Müsgen, P., Pätz, H. W., Schäfer, H. J., Schmitz, T., and Volz-Thomas, A.: Peroxy radicals during BERLIOZ at Pabstthum: Measurements, radical budgets and ozone production, J. Geophys. Res.-Atmos., 108, 2003.

Monks, P. S., Archibald, A. T., Colette, A., Cooper, O., Coyle, M., Derwent, R., Fowler, D., Granier, C., Law, K. S., Mills, G. E., Stevenson, D. S., Tarasova, O., Thouret, V., von Schneidemesser, E., Sommariva, R., Wild, O., and Williams, M. L.: Tropospheric ozone and its precursors from the urban to the global scale from air quality to short-lived climate forcer, Atmos. Chem. Phys., 15, 8889-8973, 10.5194/acp-15-8889-2015, 2015.

Nakashima, Y., Kamei, N., Kobayashi, S., and Kajii, Y.: Total OH reactivity and VOC analyses for gasoline vehicular exhaust with a chassis dynamometer, Atmos. Environ., 44, 468-475, https://doi.org/10.1016/j.atmosenv.2009.11.006, 2010.

Nakashima, Y., Kato, S., Greenberg, J., Harley, P., Karl, T., Turnipseed, A., Apel, E., Guenther, A., Smith, J., and Kajii, Y.: Total OH reactivity measurements in ambient air in a southern Rocky mountain ponderosa pine forest during BEACHON-SRM08 summer campaign, Atmos. Environ., 85, 1-8, https://doi.org/10.1016/j.atmosenv.2013.11.042, 2014.

Nölscher, A. C., Yañez-Serrano, A. M., Wolff, S., de Araujo, A. C., Lavrič, J. V., Kesselmeier, J., and Williams, J.: Unexpected seasonality in quantity and composition of Amazon rainforest air reactivity, Nature Communications, 7, 10383, 10.1038/ncomms10383, 2016.

Paoletti, E., De Marco, A., Beddows, D. C., Harrison, R. M., and Manning, W. J.: Ozone levels in European and USA cities are increasing more than at rural sites, while peak values are decreasing, Environmental Pollution, 192, 295-299, 2014.

Praplan, A. P., Tykka, T., Chen, D., Boy, M., Taipale, D., Vakkari, V., Zhou, P. T., Petaja, T., and Hellen, H.: Long-term total OH reactivity measurements in a boreal forest, Atmos. Chem. Phys., 19, 14431-14453, 10.5194/acp-19-14431-2019, 2019.

Sadanaga, Y., Yoshino, A., Kato, S., and Kajii, Y.: Measurements of OH reactivity and photochemical ozone production in the urban atmosphere, Environ. Sci. Technol., 39, 8847-8852, 2005.

Sanchez, D., Seco, R., Gu, D., Guenther, A., Mak, J., Lee, Y., Kim, D., Ahn, J., Blake, D., Herndon, S., Jeong, D., Sullivan, J. T., McGee, T., Park, R., and Kim, S.: Contributions to OH reactivity from unexplored volatile organic compounds measured by PTR-ToF-MS – a case study in a suburban forest of the Seoul metropolitan area during the Korea–United States Air Quality Study (KORUS-AQ) 2016, Atmos. Chem. Phys., 21, 6331-6345, 10.5194/acp-21-6331-2021, 2021.

Sekimoto, K., Li, S.-M., Yuan, B., Koss, A., Coggon, M., Warneke, C., and de Gouw, J.: Calculation of the sensitivity of proton-transfer-reaction mass spectrometry (PTR-MS) for organic trace gases using molecular properties, International Journal of Mass Spectrometry, 421, 71-94, 10.1016/j.ijms.2017.04.006, 2017.

Shetter, R. E., and Müller, M.: Photolysis frequency measurements using actinic flux spectroradiometry during the PEM-Tropics mission: Instrumentation description and some results, J. Geophys. Res.-Atmos., 104, 5647-5661, https://doi.org/10.1029/98JD01381, 1999.

Shirley, T. R., Brune, W. H., Ren, X., Mao, J., Lesher, R., Cardenas, B., Volkamer, R., Molina, L. T., Molina, M. J., Lamb, B., Velasco, E., Jobson, T., and Alexander, M.: Atmospheric oxidation in the Mexico City Metropolitan Area (MCMA) during April 2003, Atmos. Chem. Phys., 6, 2753-2765, 10.5194/acp-6-2753-2006, 2006.

Sillman, S., Logan, J. A., and Wofsy, S. C.: The sensitivity of ozone to nitrogen oxides and hydrocarbons in regional ozone episodes, J. Geophys. Res.-Atmos., 95, 1837-1851, 1990.

Sinha, V., Williams, J., Crowley, J., and Lelieveld, J.: The Comparative Reactivity Method–a new tool to measure total OH Reactivity in ambient air, Atmos. Chem. Phys., 8, 2213-2227, 2008.

Song, K., Gong, Y., Guo, S., Lv, D., Wang, H., Wan, Z., Yu, Y., Tang, R., Li, T., Tan, R., Zhu, W., Shen, R., and Lu, S.: Investigation of partition coefficients and fingerprints of atmospheric gas- and particle-phase intermediate volatility and semi-volatile organic compounds using pixel-

based approaches, Journal of Chromatography A, 1665, 462808, https://doi.org/10.1016/j.chroma.2022.462808, 2022.

Stewart, G. J., Nelson, B. S., Acton, W. J. F., Vaughan, A. R., Farren, N. J., Hopkins, J. R., Ward, M. W., Swift, S. J., Arya, R., Mondal, A., Jangirh, R., Ahlawat, S., Yadav, L., Sharma, S. K., Yunus, S. S. M., Hewitt, C. N., Nemitz, E., Mullinger, N., Gadi, R., Sahu, L. K., Tripathi, N., Rickard, A. R., Lee, J. D., Mandal, T. K., and Hamilton, J. F.: Emissions of intermediate-volatility and semi-volatile organic compounds from domestic fuels used in Delhi, India, Atmos. Chem. Phys., 21, 2407-2426, 10.5194/acp-21-2407-2021, 2021.

Tonnesen, G. S., and Dennis, R. L.: Analysis of radical propagation efficiency to assess ozone sensitivity to hydrocarbons and NOx: 1. Local indicators of instantaneous odd oxygen production sensitivity, J. Geophys. Res.-Atmos., 105, 9213-9225, 2000.

Wang, C., Yuan, B., Wu, C., Wang, S., Qi, J., Wang, B., Wang, Z., Hu, W., Chen, W., Ye, C., Wang, W., Sun, Y., Wang, C., Huang, S., Song, W., Wang, X., Yang, S., Zhang, S., Xu, W., Ma, N., Zhang, Z., Jiang, B., Su, H., Cheng, Y., Wang, X., and Shao, M.: Measurements of higher alkanes using NO+ chemical ionization in PTR-ToF-MS: important contributions of higher alkanes to secondary organic aerosols in China, Atmospheric Chemistry and Physics, 20, 14123-14138, 10.5194/acp-20-14123-2020, 2020a.

Wang, H., Zhang, X., and Chen, Z.: Development of DNPH/HPLC method for the measurement of carbonyl compounds in the aqueous phase: applications to laboratory simulation and field measurement, Environmental Chemistry, 6, 389-397, https://doi.org/10.1071/EN09057, 2009.

Wang, M., Zeng, L., Lu, S., Shao, M., Liu, X., Yu, X., Chen, W., Yuan, B., Zhang, Q., and Hu, M.: Development and validation of a cryogen-free automatic gas chromatograph system (GC-MS/FID) for online measurements of volatile organic compounds, Anal. Methods, 6, 9424-9434, 2014.

Wang, Q. Q., Shao, M., Liu, Y., William, K., Paul, G., Li, X. H., Liu, Y. A., and Lu, S. H.: Impact of biomass burning on urban air quality estimated by organic tracers: Guangzhou and Beijing as cases, Atmos. Environ., 41, 8380-8390, 10.1016/j.atmosenv.2007.06.048, 2007.

Wang, W., Li, X., Shao, M., Hu, M., Zeng, L., Wu, Y., and Tan, T.: The impact of aerosols on photolysis frequencies and ozone production in Beijing during the 4-year period 2012–2015, Atmos. Chem. Phys., 19, 9413-9429, 10.5194/acp-19-9413-2019, 2019.

Wang, W., Parrish, D. D., Li, X., Shao, M., Liu, Y., Mo, Z., Lu, S., Hu, M., Fang, X., and Wu, Y.: Exploring the drivers of the increased ozone production in Beijing in summertime during 2005–2016, Atmos. Chem. Phys., 20, 15617-15633, 2020b.

Wang, W., Parrish, D. D., Wang, S., Bao, F., Ni, R., Li, X., Yang, S., Wang, H., Cheng, Y., and Su, H.: Long-term trend of ozone pollution in China during 2014–2020: distinct seasonal and spatial characteristics and ozone sensitivity, Atmos. Chem. Phys., 22, 8935-8949, 10.5194/acp-22-8935-2022, 2022.

Wu, C., Wang, C., Wang, S., Wang, W., Yuan, B., Qi, J., Wang, B., Wang, H., Wang, C., and Song, W.: Measurement report: Important contributions of oxygenated compounds to emissions and chemistry of volatile organic compounds in urban air, Atmos. Chem. Phys., 20, 14769-14785, 2020.

Wu, Y., Yang, Y. D., Shao, M., and Lu, S. H.: Missing in total OH reactivity of VOCs from gasoline evaporation, Chinese Chemical Letters, 26, 1246-1248, 10.1016/j.cclet.2015.05.047, 2015.

Xie, X., Shao, M., Liu, Y., Lu, S., Chang, C.-C., and Chen, Z.-M.: Estimate of initial isoprene contribution to ozone formation potential in Beijing, China, Atmos. Environ., 42, 6000-6010, 2008.

Xu, R., Li, X., Dong, H., Lv, D., Kim, N., Yang, S., Wang, W., Chen, J., Shao, M., and Lu, S.: Field observations and quantifications of atmospheric formaldehyde partitioning in gaseous and particulate phases, Sci. Total Environ., 808, 152122, 2022.

Yang, Y., Liao, H., and Lou, S.: Increase in winter haze over eastern China in recent decades: Roles of variations in meteorological parameters and anthropogenic emissions, J. Geophys. Res.-Atmos., 121, 13,050-013,065, https://doi.org/10.1002/2016JD025136, 2016a.

Yang, Y., Shao, M., Wang, X., Nölscher, A. C., Kessel, S., Guenther, A., and Williams, J.: Towards a quantitative understanding of total OH reactivity: A review, Atmos. Environ., 134, 147-161, 2016b.

Yang, Y., Shao, M., Keßel, S., Li, Y., Lu, K., Lu, S., Williams, J., Zhang, Y., Zeng, L., Nölscher, A. C., Wu, Y., Wang, X., and Zheng, J.: How the OH reactivity affects the ozone production efficiency: case studies in Beijing and Heshan, China, Atmos. Chem. Phys., 17, 7127-7142, 10.5194/acp-17-7127-2017, 2017.

Yoshino, A., Sadanaga, Y., Watanabe, K., Kato, S., Miyakawa, Y., Matsumoto, J., and Kajii, Y.: Measurement of total OH reactivity by laser-induced pump and probe technique—comprehensive observations in the urban atmosphere of Tokyo, Atmos. Environ., 40, 7869-7881, https://doi.org/10.1016/j.atmosenv.2006.07.023, 2006.

Yu, Y., Cheng, P., Li, H., Yang, W., Han, B., Song, W., Hu, W., Wang, X., Yuan, B., Shao, M., Huang, Z., Li, Z., Zheng, J., Wang, H., and Yu, X.: Budget of nitrous acid (HONO) at an urban site in the fall season of Guangzhou, China, Atmos. Chem. Phys., 22, 8951-8971, 10.5194/acp-22-8951-2022, 2022.

Yuan, B., Chen, W., Shao, M., Wang, M., Lu, S., Wang, B., Liu, Y., Chang, C.-C., and Wang, B.: Measurements of ambient hydrocarbons and carbonyls in the Pearl River Delta (PRD), China, Atmos. Res., 116, 93-104, 2012.

Yuan, B., Hu, W., Shao, M., Wang, M., Chen, W., Lu, S., Zeng, L., and Hu, M.: VOC emissions, evolutions and contributions to SOA formation at a receptor site in eastern China, Atmos. Chem. Phys., 13, 8815-8832, 2013.

Yuan, B., Koss, A. R., Warneke, C., Coggon, M., Sekimoto, K., and de Gouw, J. A.: Proton-Transfer-Reaction Mass Spectrometry: Applications in Atmospheric Sciences, Chemical Reviews, 117, 13187-13229, 10.1021/acs.chemrev.7b00325, 2017.

631

632
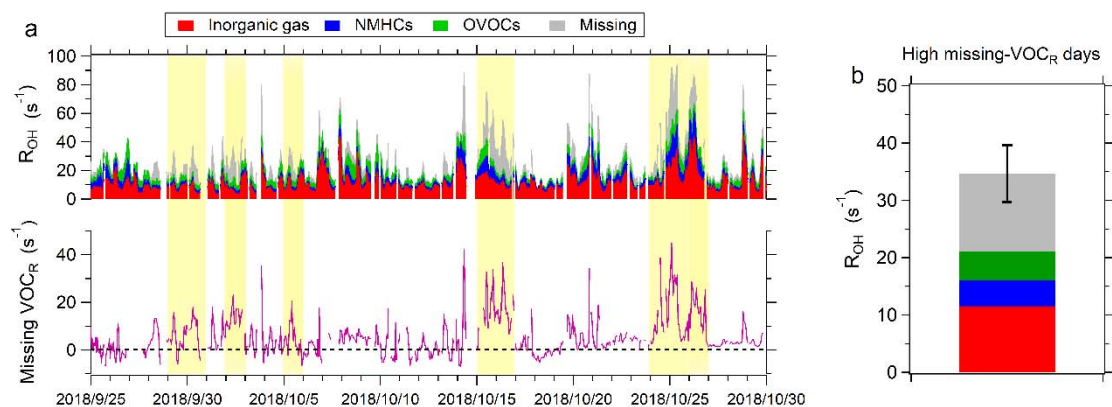
Figure 1. The level of missing VOC$_R$ during the measurements in Guangzhou. (a) Time series of measured R$_{OH}$ and calculated R$_{OH}$ from all measured reactive gases in Guangzhou. Yellow background represents the high missing-VOC$_R$ days with missing VOC$_R$ accounting for more than 30% of total R$_{OH}$. (b) Contributions of different compositions to R$_{OH}$ in high missing-VOC$_R$ days. The error bar represents standard deviation of missing VOC$_R$.

639

640

641

644
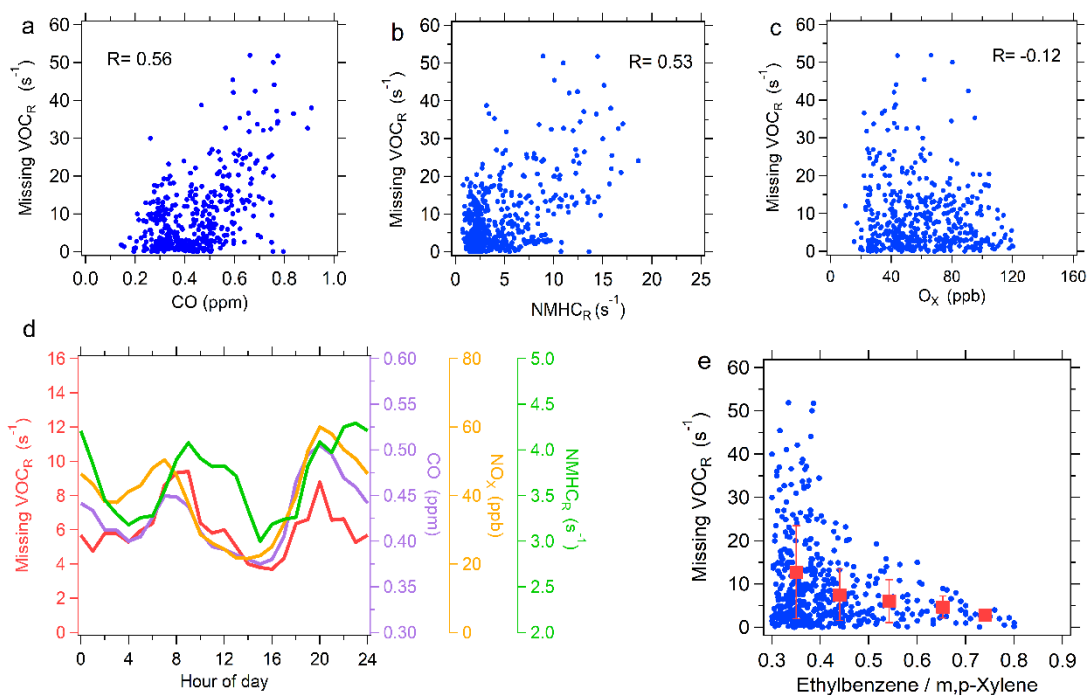
Figure 2. Correlation of missing VOC$_R$ with major tracers during the whole measurement period. (a-c) Correlation of missing VOC$_R$ with CO, OH reactivity of NMHCs (NMHC$_R$) and O$_X$. Each point represents hourly data. (d) Diurnal variations in missing VOC$_R$, CO, NO$_X$ and NMHCs. (e) The dependence of missing VOC$_R$ on ethylbenzene to m, p-xylene ratio. The red squares indicate the mean values of missing VOCR in different ranges of ethylbenzene/m,p-xylene with classification width of 0.1, and the error bars represent standard deviation.

652

653

654

655
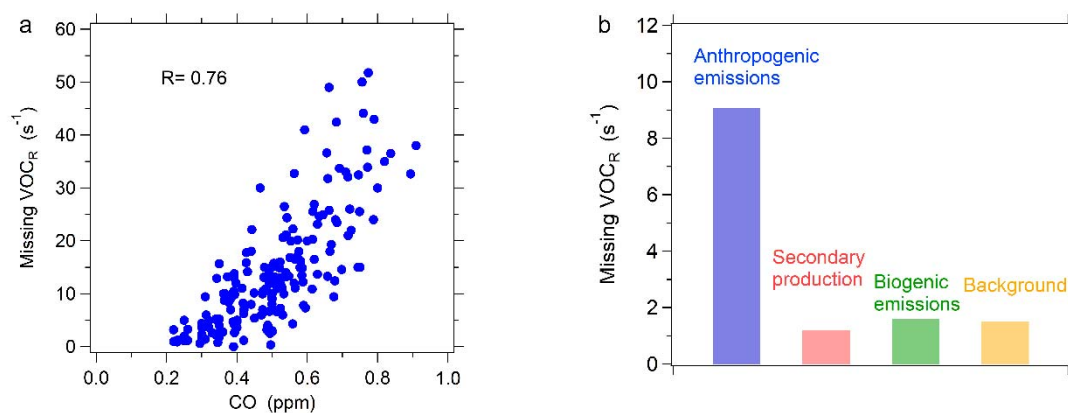
Figure 3. The source apportionment of missing VOC$_R$ in high missing-VOC$_R$ days.

(a) Correlation of missing VOC$_R$ with CO. Each point represents hourly data. (b) Contributions of different sources to missing VOC$_R$ according to the MLR.

659
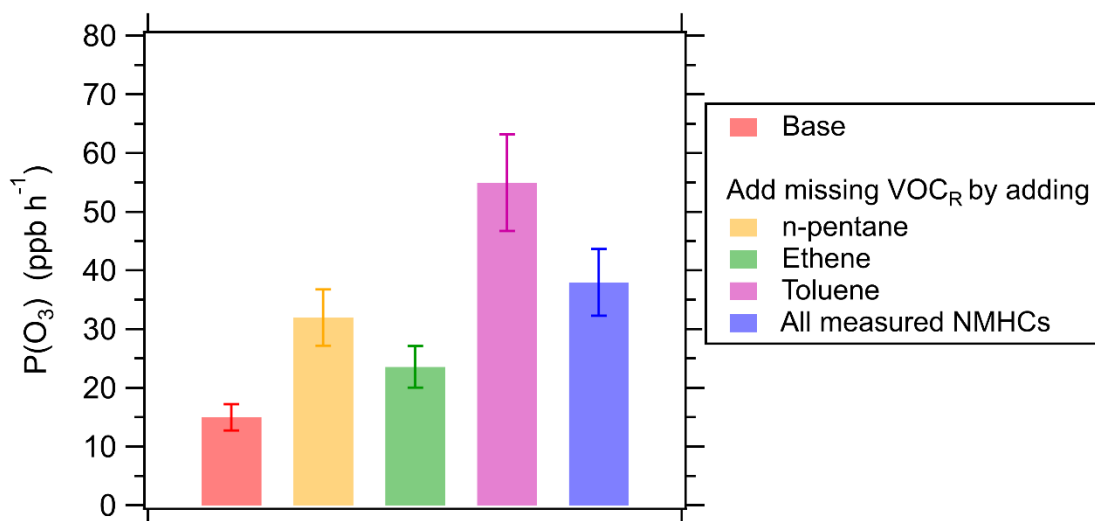
Figure 4. Simulated daytime mean $P(O_3)$ for the base scenario (without missing VOC$_R$) and the scenario considering missing VOC$_R$, respectively, in high-missing VOC$_R$ days. The missing VOC$_R$ is considered by adding individual species (n-pentane, ethene or toluene) or increasing all measured NMHCs to compensate for the missing VOC$_R$. The error bar represents standard deviation of $P(O_3)$ induced by the uncertainty of missing VOC$_R$.
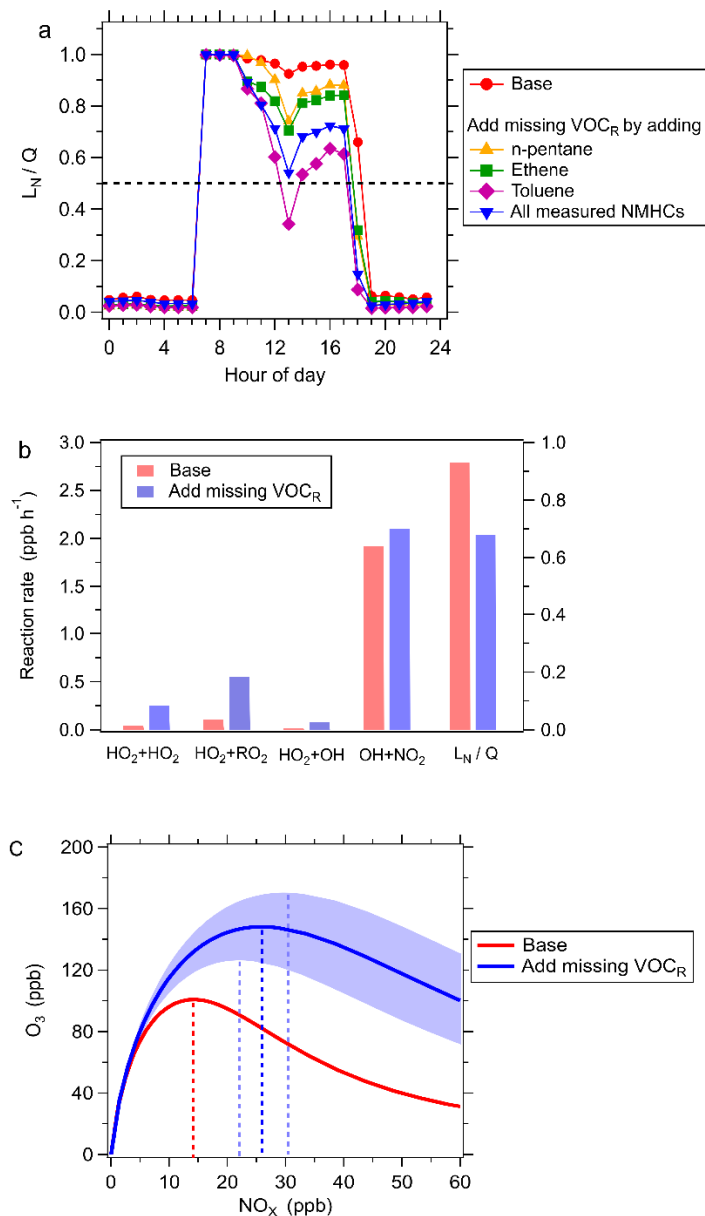
Figure 5. The impact of missing VOC$_R$ on O$_3$ sensitivity for the high-missing VOC$_R$ days. (a) Diurnal variations in L$_N$/Q for the base scenario and the scenarios considering missing VOC$_R$. The missing VOC$_R$ is considered by adding individual species (n-pentane, ethene or toluene) or increasing all measured NMHCs to fill the missing VOC$_R$. The dashed line represents the threshold value of L$_N$/Q that distinguishes VOC-limited and NO$_X$-limited regimes. (b) The averages of radical sinks in the afternoon (12:00-18:00) for the base scenario (red bar) and the scenario considering missing VOC$_R$ (blue bar) by increasing all measured NMHCs to fill the missing VOC$_R$. (c) Model-simulated dependence of daily peak O$_3$ concentrations on daily mean NO$_X$ concentrations for the

base scenario (red curve) and the scenario considering missing VOC_R (blue curve) by increasing all measured NMHCs to fill the missing VOC_R. The dashed lines parallel to Y-axis represent the threshold of NO_X levels to distinguish between VOC-limited and NO_X-limited regimes. The shaded area represents standard deviation induced by the uncertainty in missing VOC_R.